ME503

Project Report

Intake and Exhaust Port Simulations

Akira Madono

Introduction

One of the critical performance factors for a four stroke cycle internal combustion engine is the volumetric efficiency, η_v. It is expressed as

$$\eta_v = \frac{2\dot{m}_a}{\rho_{a,i} V_d N} \tag{1}$$

where $\dot{m}_a$ is the mass flow rate of air, $\rho_{a,i}$ is the density of air inducted, V_d is the displacement volume, and N is the speed of the engine. It is the volumetric flow rate of air inducted into the engine over the volumetric flow rate of air displaced by the pistons. It also represents the ratio of air that is trapped in the piston during the intake displacement stroke. The more air that can be trapped in the piston during the intake stroke, the better the performance of the engine. Since the volumetric flow rate of air displaced by the pistons is fixed by cylinder geometry, we are thus seeking to maximize $\dot{m}_a$.

One of the main reasons that air flow is reduced is due to the valves at the intake and exhaust ports that restrict the flow of air, and cause significant friction-based pressure losses. Many geometry parameters of the intake and exhaust ports can be varied in order to maximize $\dot{m}_a$. These include but are not limited to the bending radius of the ports, the diameters of the ports, the diameter of the valves, width of the valve stems, and the seat angle of the valves. Because of the need to distribute intake and exhaust flow for multi-cylinder engines, the geometry of the manifolds also influence $\dot{m}_a$.

In this project, we hope to simulate the quasi-static effects of port flow through the intake and exhaust valves. These are distinguished from transient effects that arise from a range of dynamically varying processes including various valve lift profiles (e.g. timing of cam shafts), and a host of combustion events. What we mean by quasi-static, is that we are observing effects that

are independent of the engine speed. In other words, we are observing the steady-state flow behavior at different valve lift heights. The simulation will be a computational fluid dynamics (CFD) simulation in Ansys FLUENT.

The most ideal scenario for flow with area restriction is flow with area change through a converging diverging nozzle (CD nozzle) neglecting both friction effects and heat transfer effects. In gas dynamics flow language, this is flow with area change neglecting Fanno flow and Rayleigh flow respectively. Another significant difference between real valve flow and flow through CD nozzles is the sudden area expansion when the flow exits the valve and enters the piston. These significant differences area captured by the discharge coefficient C_D. It is defined as

$$C_D = \frac{actual\ mass\ flow\ rate}{ideal\ mass\ flow\ rate} \tag{2}$$

In this case the ideal mass flow rate is the mass flow rate through a CD nozzle. Obviously, the most ideal valve will be a CD nozzle, in which case the C_D value will be 1. The connection to our volumetric flow rate discussion earlier, is that as the C_D value increases, the actual mass flow rate increases. Thus the volumetric flow rate also increases. In order to understand how C_D values are calculated, we must understand how ideal mass flow rates are actually calculated. Thus, the natural starting point is to derive the mass flow rate through an ideal CD nozzle.

Theory

Deriving Mass Flow Rates

The mass specific enthalpy h is the internal and flow energy possessed by a fluid on a per mass basis. The idea of stagnation is to introduce some equivalence in specific enthalpy states between moving and non-moving fluids. This gives rise to the definition of stagnation enthalpy h_0.

$$h_0 \equiv h + \frac{v^2}{2} \tag{3}$$

It is the specific enthalpy a fluid would possess if it could be slowed down in adiabatic and reversible way. This isentropic expansion, is imagined to occur in an infinitely smooth chamber which expands from an initial cross sectional area to an infinite area. In our case, we will be mainly considering air, and as such, we will assume air to act as an ideal gas. Air can often be assumed to behave like an ideal gas, so this assumption is valid. This assumption means that we can treat the specific heat as constant. As such,

$$h = c_p T \tag{4}$$

Substituting into Eq. (4)

$$c_p T_0 = c_p T + \frac{v^2}{2} \tag{5}$$

The stagnation temperature is thus

$$T_0 \equiv T + \frac{v^2}{2c_p} \tag{6}$$

The ideal gas assumption also allows us to assume a constant γ, the specific gas ratio, and the Eq. of state,

$$p = \rho R T \tag{7}$$

We will use these two facts to derive an expression for pressure changes with respect to temperature changes through an isentropic expansion. Invoking the first law for a closed system,

$$\delta q + \delta w = du \tag{8}$$

We know that reversible work done on a closed system by volume change is,

$$\delta w = -p\, dv \tag{9}$$

But we are neglecting heat transfer δq. Thus, substituting Eq. (9) into Eq. (8)

$$du = -p\, dv \tag{10}$$

Also, the definition of specific enthalpy is given as,

$$h \equiv u + pV \tag{11}$$

Thus, the differential of specific enthalpy is,

$$dh = du + v\, dp + p\, dv \tag{12}$$

Substituting Eq. (10) into Eq. (12),

$$dh = -p\, dv + v\, dp + p\, dv = v\, dp \tag{13}$$

We also have the ideal gas relations

$$\begin{aligned} dh &= c_p dT \\ du &= c_v dT \end{aligned} \tag{14}$$

We can thus identify from Eq. (14) that

$$\frac{dh}{du} = \frac{c_p}{c_v} \tag{15}$$

We can also see from the definition of γ, Eq. (10), and Eq. (13)

$$\gamma \equiv \frac{c_p}{cv} = \frac{dh}{du} = \frac{v\, dp}{-p\, dv} \tag{16}$$

We then integrate Eq. (16) for an isentropic flow assuming $\gamma = const.$, as it is for an ideal gas.

$$-\gamma \int \frac{dv}{v} = \int \frac{dp}{p} \tag{17}$$

If we designate pressure at an area with th to a stagnation state 0

$$\frac{p_0}{p_{th}} = \left(\frac{v_{th}}{v_0}\right)^{\gamma} \tag{18}$$

If we invoke the Eq. of state, Eq. (7), we can represent Eq. (18) by

$$\frac{T_{th}}{T_0} = \left(\frac{p_{th}}{p_0}\right)^{\frac{\gamma-1}{\gamma}} \tag{19}$$

The Mach number is defined as

$$M \equiv \frac{V}{a} = \frac{V}{\sqrt{\gamma RT}} \tag{20}$$

where V is the speed of the gas, and a is the speed of sound in that gas. If we substitute this definition into Eq. (6), we have,

$$\frac{T_0}{T_{th}} = 1 + \frac{\gamma R}{2c_p}M^2 = 1 + \frac{R}{2c_v}M^2 \tag{21}$$

But since,

$$c_p = c_v + R \tag{22}$$

We can combine with the definition of γ to see that

$$\gamma - 1 = \frac{R}{c_v} \tag{23}$$

Substituting Eq. (23) into Eq. (21),

$$\frac{T_0}{T_{th}} = 1 + \frac{\gamma - 1}{2}M^2 \tag{24}$$

We can combine with the isentropic expansion relation in Eq. (19) to show that

$$\frac{p_0}{p_{th}} = \left(1 + \frac{\gamma - 1}{2}M^2\right)^{\frac{\gamma}{\gamma-1}} \tag{25}$$

From here deriving the ideal mass flow rate for an isentropic expansion follows through in a predictable manner. We start with the definition of the mass flow rate.

$$\dot{m} = \rho A V \tag{26}$$

Substituting in the equation of state in Eq. (7) for ρ and the Mach number definition given in Eq. (20),

$$\dot{m} = \frac{p_{th}}{RT} A M \sqrt{\gamma R T} \tag{27}$$

Letting $p = p_{th}$, and substituting Eq. (25) into Eq. (27),

$$\dot{m} = \frac{p_0 / \left(1 + \frac{\gamma - 1}{2} M^2\right)^{\frac{\gamma}{\gamma - 1}}}{RT} A M \sqrt{\gamma R T} \tag{28}$$

Letting $T = T_{th}$ and substituting Eq. (24) into Eq. 28)

$$\dot{m} = A p_0 \sqrt{\frac{\gamma}{R T_0}} M \left(1 + \frac{\gamma - 1}{2} M^2\right)^{-\frac{\gamma + 1}{2(\gamma - 1)}} \tag{29}$$

Eq. (25) can be rewritten as,

$$M^2 = \left(\frac{2}{\gamma - 1}\right)\left(\frac{p_0}{p_{th}}^{\frac{\gamma - 1}{\gamma}} - 1\right) \tag{30}$$

This permits the rearrangement of Eq. (29) as,

$$\dot{m}_{ideal} = A p_0 \sqrt{\frac{\gamma}{R T_0}} \left(\frac{p_{th}}{p_0}\right)^{\frac{1}{\gamma}} \left(\frac{2}{\gamma - 1}\left(1 - \frac{p_{th}}{p_0}^{\frac{\gamma - 1}{\gamma}}\right)\right)^{0.5} \tag{31}$$

An alternate rearranged form of Eq. (31) uses the Eq. (7) to replace knowing T_0 with knowing ρ_0.

$$\dot{m}_{ideal} = A[2\rho_0(p_0 - p_T)]^{0.5}\left\{\frac{\frac{\gamma}{\gamma-1}p_0\left[\left(\frac{p_{th}}{p_0}\right)^{\frac{2}{\gamma}} - \frac{p_{th}}{p_0}^{\frac{\gamma+1}{\gamma}}\right]}{1-\frac{p_{th}}{p_0}}\right\}^{0.5} \quad (32)$$

Note that we have denoted the mass flow rate $\dot{m}$ as *ideal* because it is for an ideal isentropic expansion. The area A is chosen arbitrarily through an area in which all the flow passes through. We chose the reference area to be

$$A = \pi L_v D_v \quad (33)$$

where L_v and D_v are the valve lift height and diameter respectively.

We can see that we can calculate the ideal mass flow rate for an isentropic expansion from a given area A. If we know the mass flow rate for the real system with the same area A, from Eq. (2), we know that we can calculate the discharge coefficient. It should also be noted that Eq. (31) is equally valid for an isentropic compression from a stagnation state p_0. Thus we have all the equations we need to study the CD nozzle and the analogous flow through the valves.

Expected Results

The general trends in pressure and density we expect will follow those for compressible gases through a CD nozzle. Pressure and density decrease towards the throat of the nozzle. Velocity will increase. The pressure and density will then rise following the throat if flow does not choke. The reference figure, Fig. 5.1 [2] explains these expectations in detail. If the flow chokes, the exhaust pipe will increase flow to supersonic levels.

For intake flow, Fig. 6-16 [1] provides expected results for the discharge coefficient C_D and qualitative expectations for flow patterns observed. Initially, as the valve rises, flow follows the path of the valve geometry seat; it has not separated. C_D then varies due to discrepancies

between flow separation occurring for real flow as opposed to the CD nozzle case in which the flow never separates. Gradually, as the valve continues to lift, the mass flow rates increase, and swirl is generated. Given that swirl is yet another irreversible process, C_D will continue to decrease.

On the exhaust side, Fig. 6-17 [1] shows that flow separation is more prevalent for high lift conditions than low lift conditions. These irreversible processes again result in decreased discharge coefficients. Also, due to the much higher pressure differentials across the valve, choking is much more likely to occur on the exhaust side.

Simulation Conditions

In order to facilitate this calculation, we will need to determine what quantities are identical for the ideal mass flow rate calculation, and the actual mass flow rate, which we will find by conducting a CFD simulation. In order to calculate $\dot{m}_{ideal}$ in Eq. (32), we need to know p_0, ρ_0, p_{th} and γ. In the ideal CD nozzle, the stagnation properties are equal at the beginning and end of the nozzle. However in reality, due to irreversible processes the downstream stagnation properties are less than the upstream stagnation properties as discussed previously.

Thus, we will use the upstream stagnation values found from the simulation. We can find p_{th} if we know the velocity at the throat since the ratio p_{th}/p_o is directly a function of Mach number. We can determine the Mach number for the simulation by examining velocity values at the throat. Thus in summary, we will be using the stagnation values ρ_0, p_0 upstream from the simulation and the velocity at the throat to calculate $\dot{m}_{ideal}$ based on Eq. (32). The actual flow rate $\dot{m}_{actual,}$ we will take directly from the simulation just downstream of the valve at the entrance of the cylinder.

One aspect of the simulation that we should also mention is temperature variation. For simulation of intake flow, setting all geometric surfaces to be 300 K makes sense, since no heating is taking place prior to combustion. Heat transfer effects are therefore negligible. However, for an exhaust simulation, we should take into account the higher temperatures that all components will be at due to combustion. Note that in both the intake and exhaust case we set all initial temperatures to a uniform value in light of the steady-state flow properties we wanted to analyze. In order to find representative values, we appealed to a reference, Fig. 6-21 [1]. That figure provides estimates for cylinder pressures and temperatures. In order to quantify the values given in Fig. 6-21 [1], we used the webplotdigizer application. Not knowing the actual valve lift profile for the engine on which that figure was based, we superimposed a typical valve lift profile with $10\ mm$ lift on the given valve opening and closing crank angles. The results are given by Figure A.1.

The remaining parameters for the simulation are as follows. Typical valve lift heights go up to $10\ mm$ for the engine geometry so we studied flow behavior from low to high values in this range. To enable flow to actually occur for intake and exhaust flows, we needed to create pressure differentials. For the intake side, we set the entrance pressure to be $1\ atm$, and the outlet of the cylinder to be $5\ kPa$ less than atmospheric. The exhaust pressure and temperature at the inlet was set according to Fig 6-21 [1] while the pressure at the exhaust side was set to $1\ atm$. All other boundaries were set to be slipwalls. That is, walls that allow for slip, but are adiabatic.

The Simulation Model

We will use a turbulence-based 3D $k-\omega$ model given that turbulence is expected in the high velocities encountered in internal combustion engines. Modeling the air as an ideal gas, we

set the specific heat to be constant. We set the grid size to be as high as possible since we knew accuracy would increase with grid size. The number of elements in the academic version of Ansys FLUENT limited the number of elements used to 512,000. Pressure was modeled with a standard scheme, while density, momentum, and energy were modeled with a second order upwind scheme. Turbulent kinetic energy and specific dissipation rate, k and ω in the model, were modeled with a first order upwind scheme.

Results

Convergence

Figure A.2 shows the typical convergence plot for the simulations. We converged the simulation such that average velocity values in a cross section of the engine cylinder did not differ more than $1x10^{-5}$ from the previous iteration.

Qualitative Results

For the intake simulation, the velocity contour plots in Figure A.3 show that flow separates from the top side of the valve and continues to follow the valve seat. This is in contrast to the valve Figures given in Fig 6-16 [1]. The velocity is also seen to reach a maximum in the narrowest section as anticipated for all lift heights. The most dramatic results are in Figure A.4. and Figure A.5. As the flow is restricted, pressure and density fall, but then as the area suddenly expands below the valve, the pressure and density do not rapidly increase. Indeed, the sudden expansion does not allow the pressure to rise to any appreciable extent. Clearly, the simulation is modeling irreversibilities present in the actual system. It is the extent of these effects that is questionable given expectations such as Fig. C-2 [1] where an appreciable rise in actual systems occurs. The

overall small change in pressure and density is consistent with the pressure differential of 5 kPa that was set.

On the exhaust side, the behavior of the system is quite different given the higher temperatures and pressure differentials involved as shown in Figure A.7. At a low valve lift, velocity reaches a maximum of approximately 530 m/s this is nearly choked flow given that Mach speed is 684 m/s at the system temperature of 1167 K. Our prediction of near choking behavior was then correct. The expected flow behavior of symmetric flow strength near the seat of the valve and the port wall are not evident in Figure A.6. This is consistent with the same deficiency in the model observed on the intake side. In the high lift scenario, as shown in Figure A.8, the high flow velocity occurs away from the valve seat in contrast to all the other simulations. This pattern also coincides with pressure appreciably rising after the valve opening as shown in Figure A.10.

Quantitative Results

As we discussed in the theory section, we wanted to calculate discharge coefficients C_D using simulated values. The calculations are shown in Table A.11 and Table A.12. Comparisons with expectations shown in Figure A.13 in trends. There is a consistent offset in C_D values from expectations. The results set up by the expected values are based on actual engine simulations as discussed in Fig. 6-16 [1]. We suspect these discrepancies are the result of not knowing the exact engine parameters for pressure differentials and geometry used in the actual experiments.

Conclusion

We derived the ideal mass flow rate for an isentropic expansion. This mass flow rate is the upper bound for actual flow through an engine's valve and port intake and exhaust system. The

design of the intake and exhaust systems is optimal with respect to volumetric efficiency when the system comes close to the adiabatic and frictionless converging diverging nozzle. Based on these theoretical foundations, we simulated 3D, steady-state, turbulent port flow for the intake and exhaust for a variety of lift heights. Assuming that the steady-state phenomena we modeled are applicable to the transient, real engine scenario, we tried to determine how accurate our simulation could be.

With the exception of the high valve lift exhaust case, flow was shown to asymmetrically each a maximum along the valve seat, not exhibiting symmetric behavior as shown in Fig. 6-16 and Fig. 6-17 [1]. In addition, the pressure and density also did not appreciably rise, with the exception of the high valve lift exhaust case. This is the likely symptom of discharge coefficients that were offset from expected values. Other inevitable sources of error include not knowing the exact dimensions of the engines and valves that were used for actual experiments. Aside from these deficiencies, our simulations were able to quantitatively model a number of common aspects of compressible flow including rapid fluctuations in velocity along the flow path as well as expected decreases in pressure and density for subsonic flow into the throat of the valve.

Future work in port flow simulations would certainly involve rectifying the qualitative discrepancies above. In addition, it would be helpful to show how changes in valve and port geometry affect results. Ways to quantitatively measure Swirl would also be helpful in characterizing irreversibility present in the actual system.

References

1. Heywood, John B. *Internal combustion engine fundamentals*. Vol. 930. New York: Mcgraw-hill, 1988.
2. Zucker, Robert D., and Oscar Biblarz. *Fundamentals of gas dynamics*. John Wiley & Sons, 2002.

Appendix

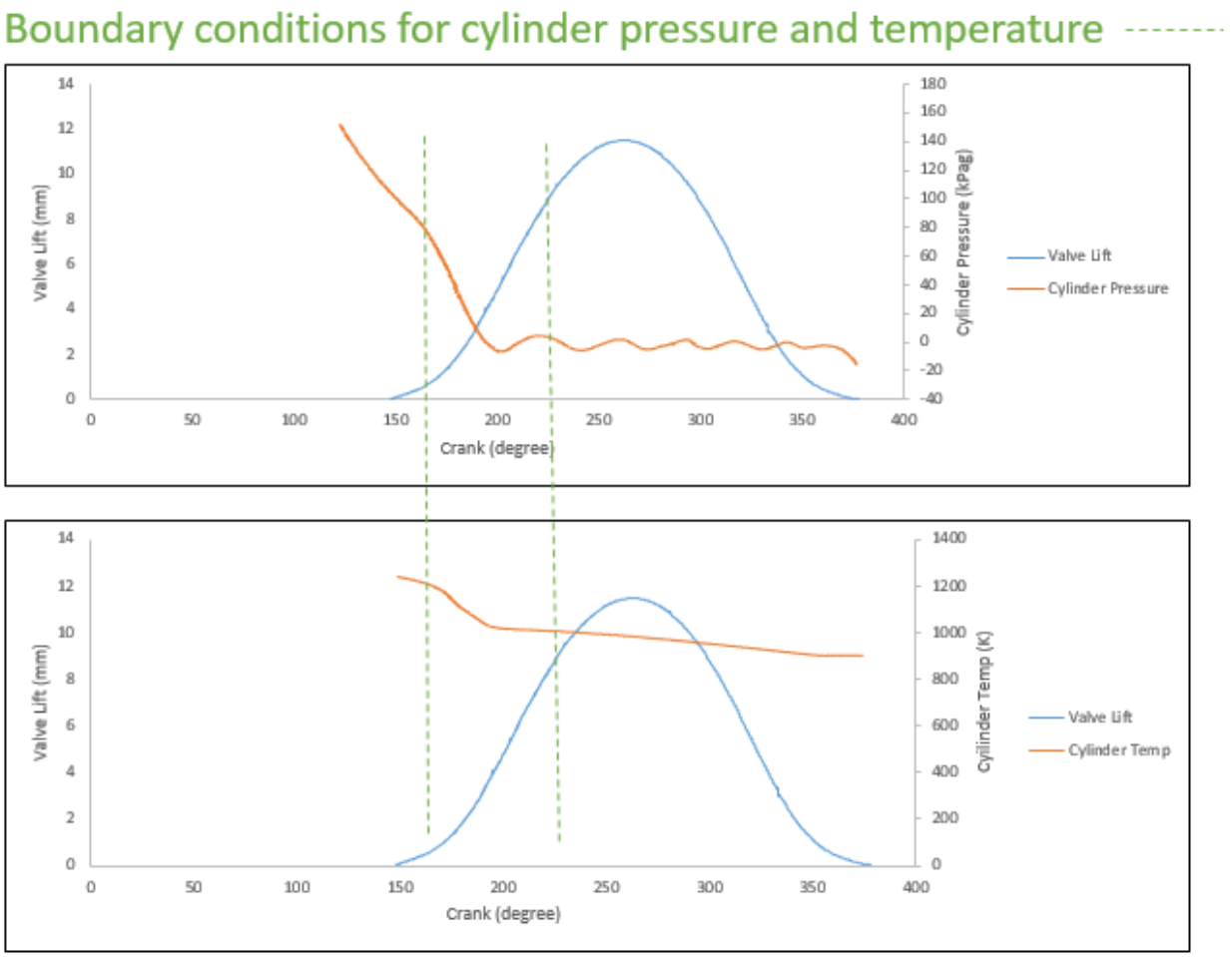

Figure A.1. Superimposing valve lift profiles with maximum lift of 10 *mm* on cylinder pressures and cylinder temperatures given in Fig. 6-21 [1].

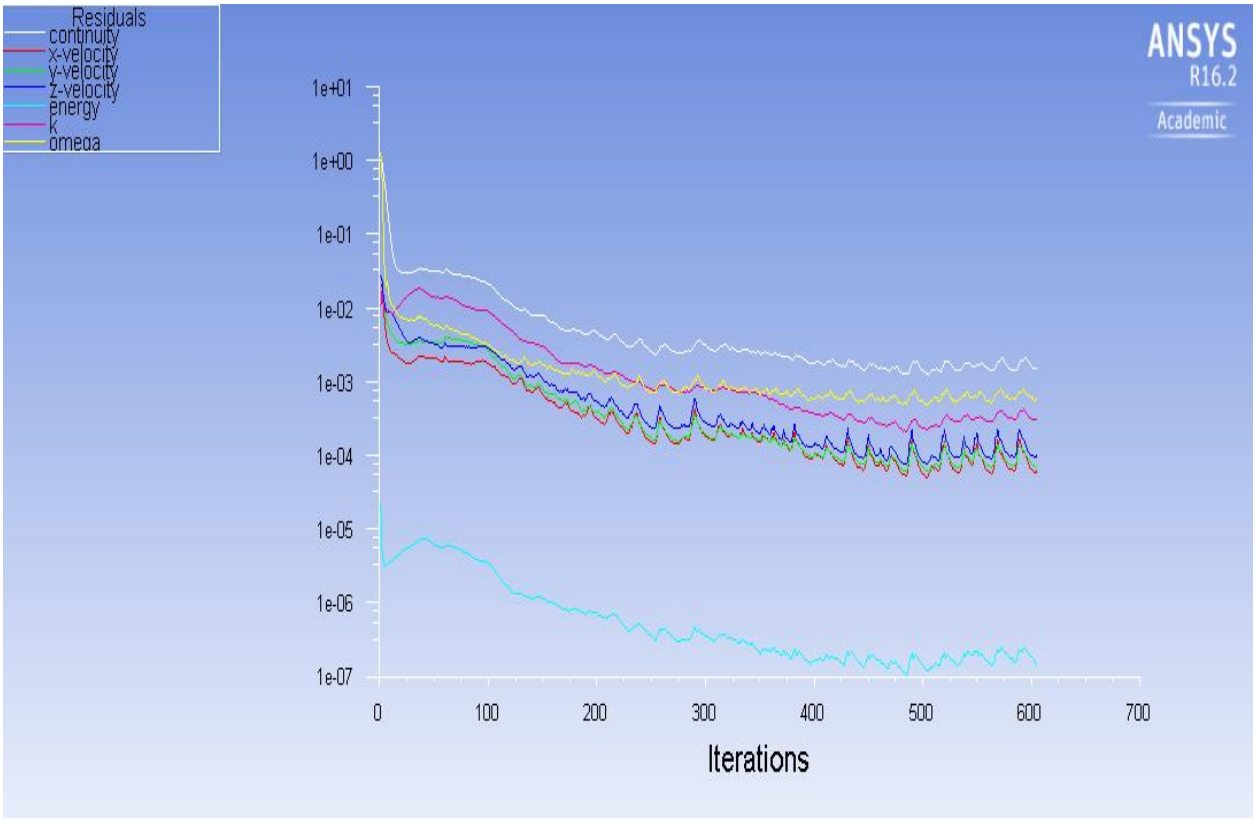

Figure A.2. Typical convergence plot.

Intake Simulation

$L_v = 2\ mm$

$\frac{L_v}{D_v} = .068$

$L_v = 4\ mm$

$\frac{L_v}{D_v} = .14$

$L_v = 10\ mm$

$\frac{L_v}{D_v} = ..34$

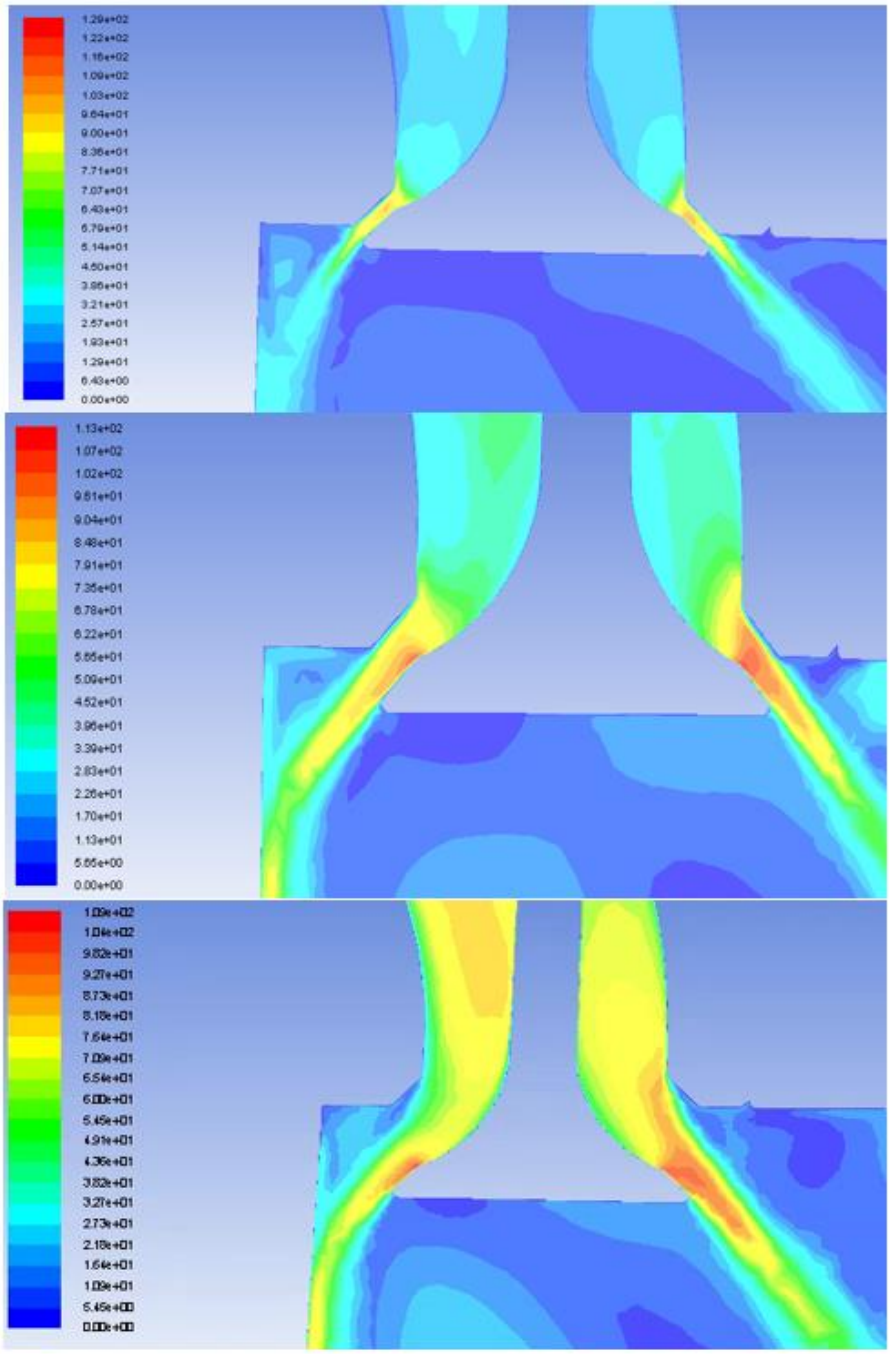

Figure A.3. Velocity contours given in m/s.

$L_v = 2\ mm$

$\frac{L_v}{D_v} = .068$

$L_v = 4\ mm$

$\frac{L_v}{D_v} = .14$

$L_v = 10\ mm$

$\frac{L_v}{D_v} = ..34$

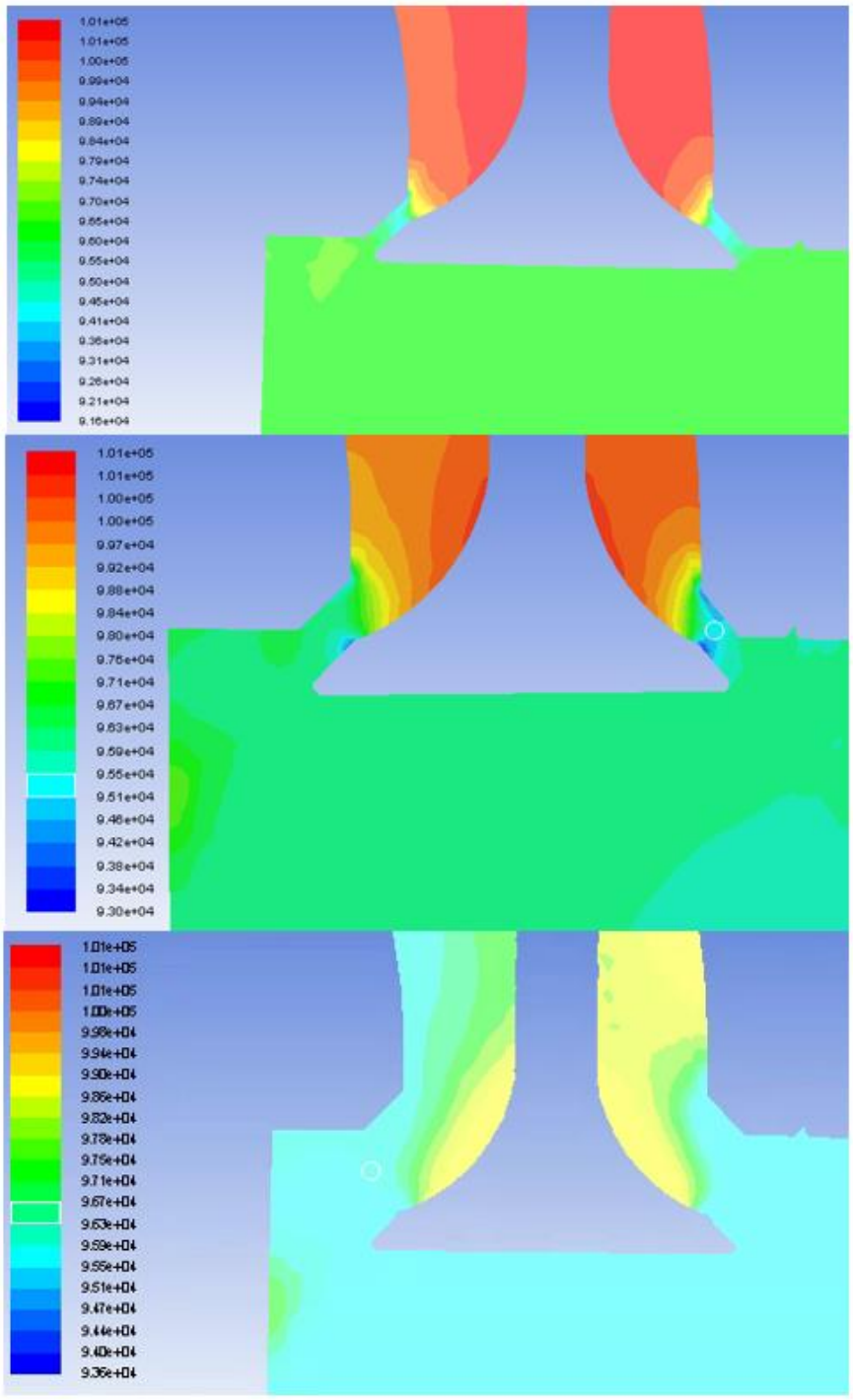

Figure A.4. Pressure contours given in Pa.

$L_v = 2\ mm$

$\frac{L_v}{D_v} = .068$

$L_v = 4\ mm$

$\frac{L_v}{D_v} = .14$

$L_v = 10\ mm$

$\frac{L_v}{D_v} = ..34$

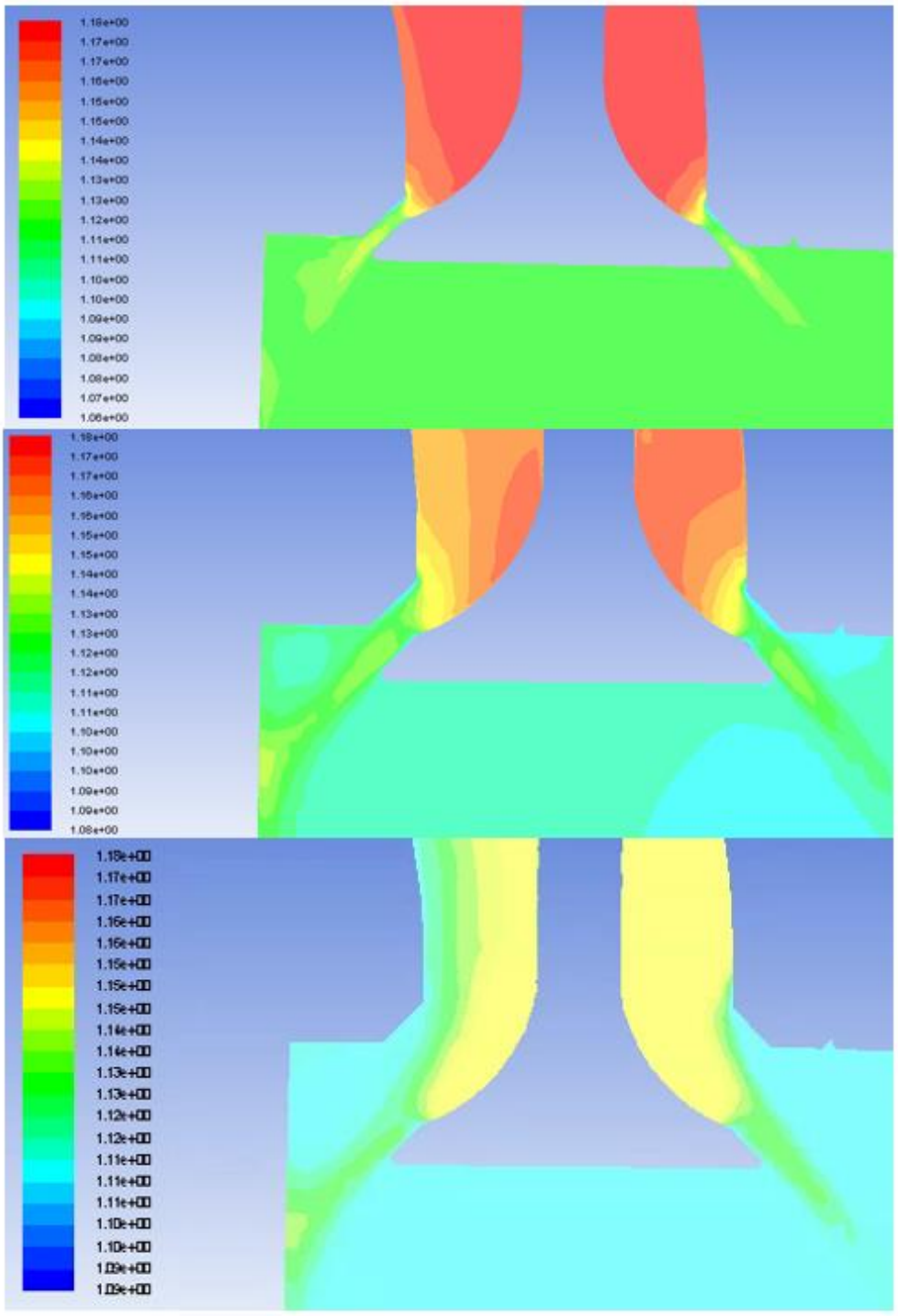

Figure A.5. Density contours given in kg/m^3.

Exhaust Simulation

Low lift scenario $Lv = 1mm$

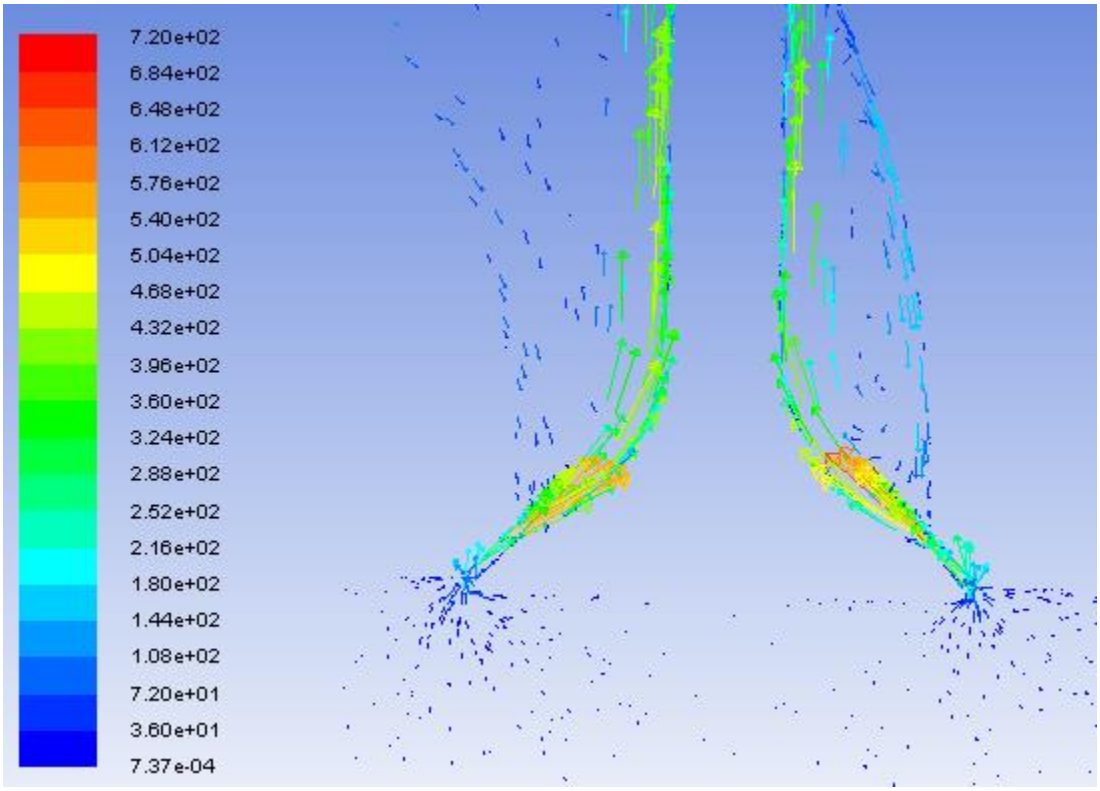

Figure A.6. Velocity vectors shown in m/s.

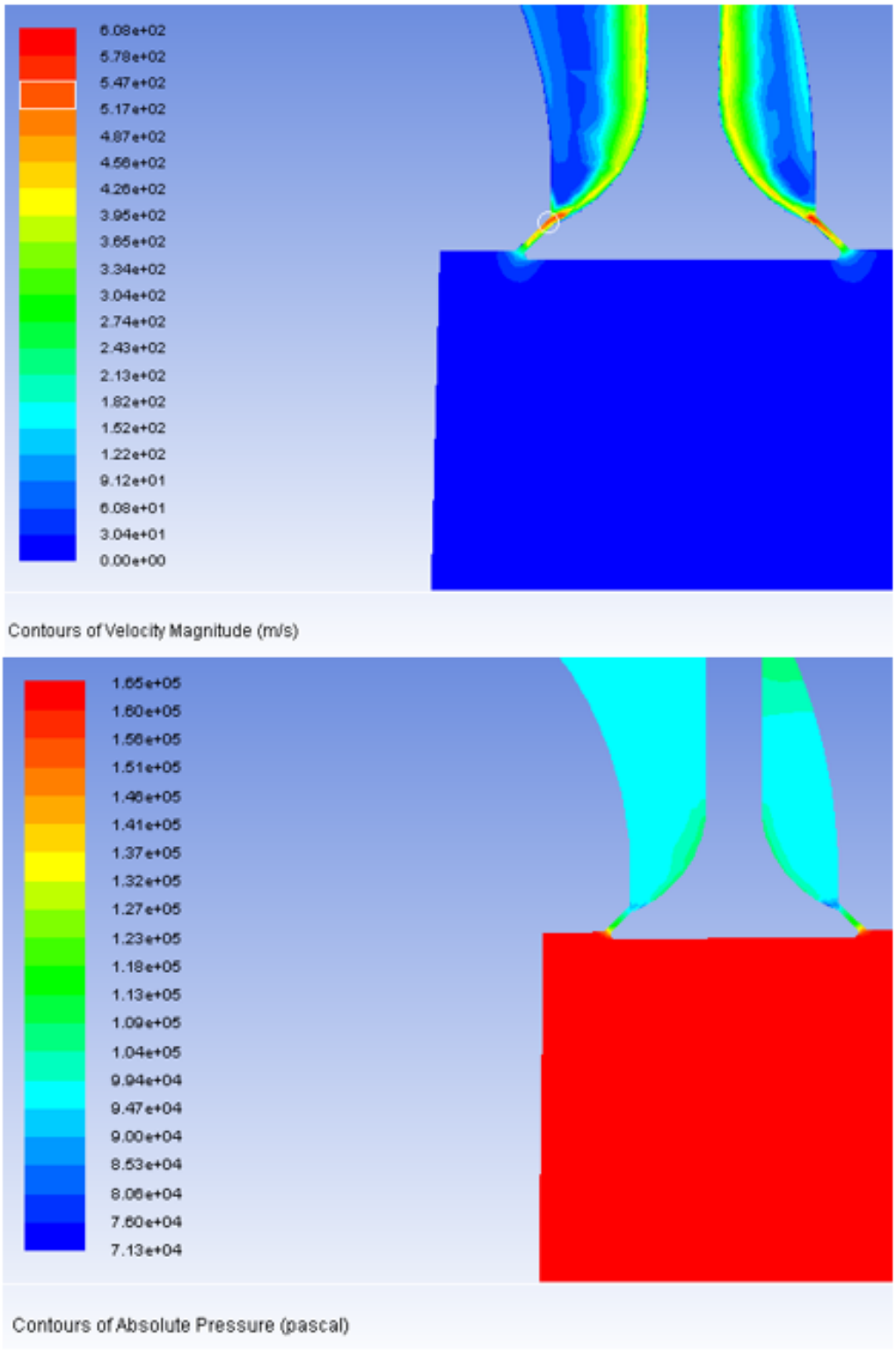

Figure A.7. Velocity and pressure contours.

High lift scenario $L_v = 8.36\ mm$

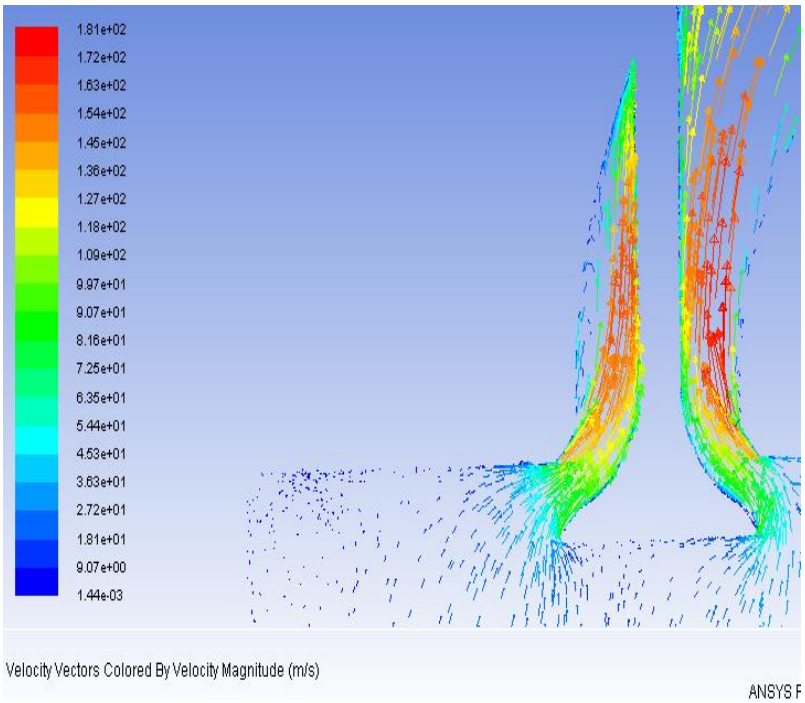

Figure A.8. Velocity vectors.

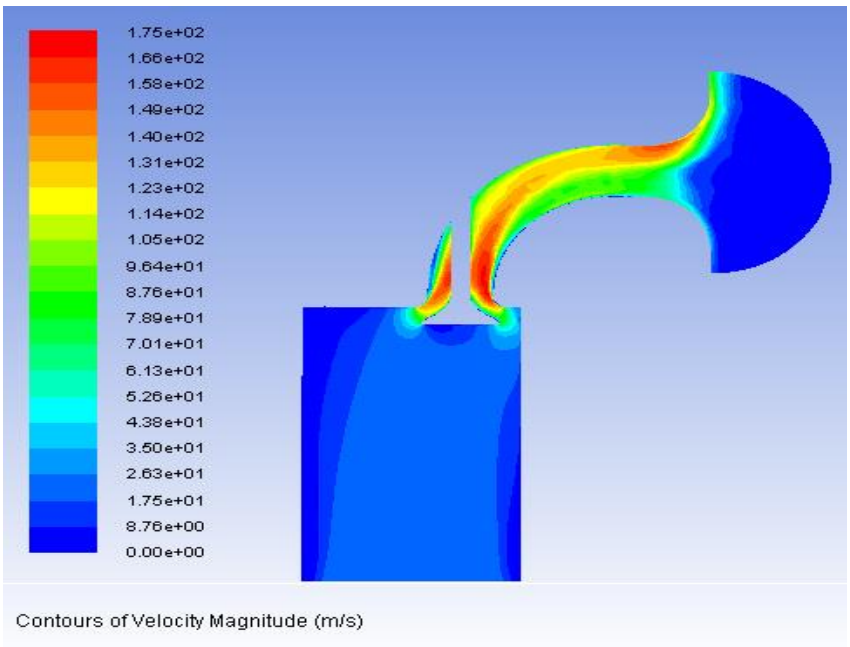

Figure A.9. Velocity contours.

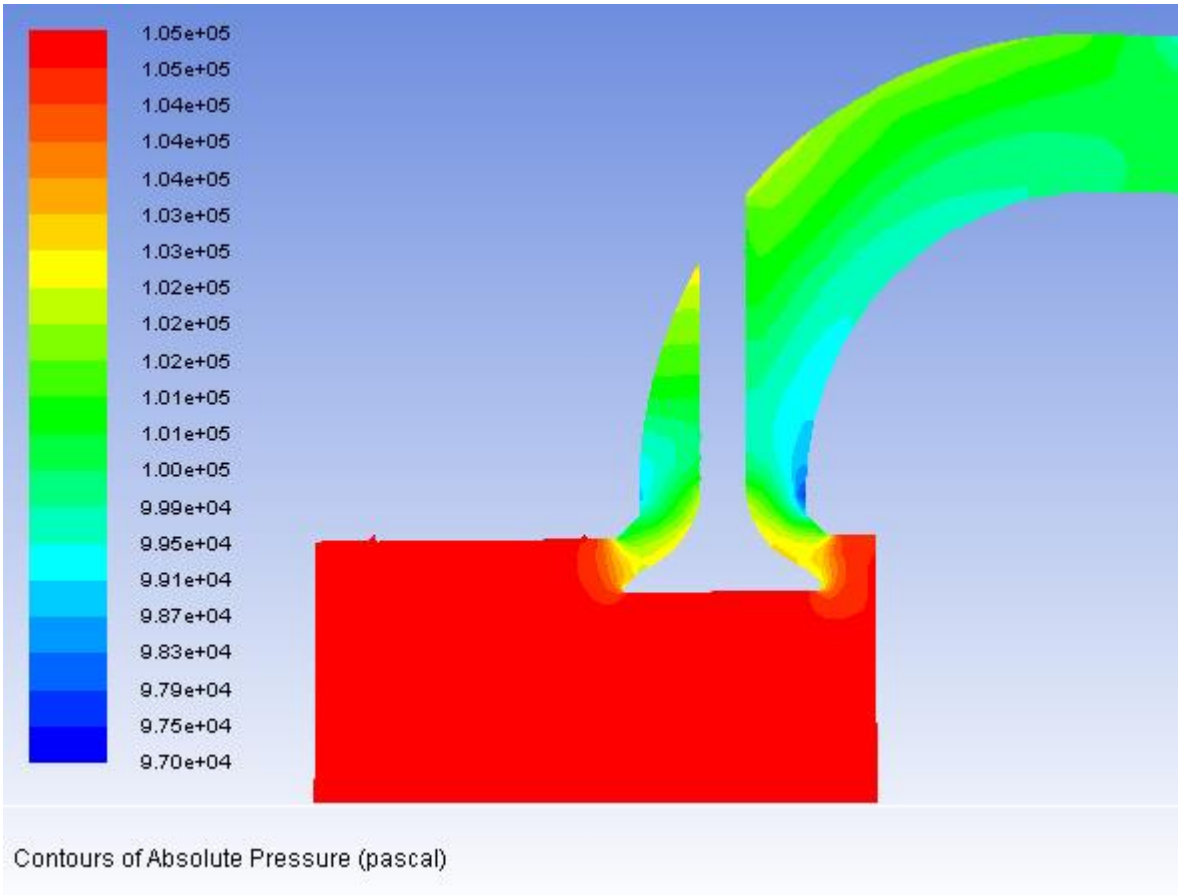

Figure A.10. Pressure contours.

Table A.11. Calculations for discharge coefficient.

$L_v\ [m]$	L_v/D_v	$V\ [m/s]$	M	$\frac{p}{p_0}$	$A\ [m^2]$
1.00E-03	3.40E-02	7.98E+01	2.30E-01	9.64E-01	9.23E-05
2.00E-03	6.81E-02	9.32E+01	2.68E-01	9.51E-01	1.85E-04
3.00E-03	1.02E-01	1.07E+02	3.08E-01	9.36E-01	2.77E-04
4.00E-03	1.36E-01	1.10E+02	3.17E-01	9.33E-01	3.69E-04
5.00E-03	1.70E-01	8.77E+01	2.53E-01	9.57E-01	4.61E-04
7.00E-03	2.38E-01	9.64E+01	2.77E-01	9.48E-01	6.46E-04
1.00E-02	3.40E-01	9.00E+01	2.59E-01	9.54E-01	9.23E-04

Table A.12. C_D calculations continued.

$L_v[m]$	$\rho_0\ [kg/m^3]$	$p_0[Pa]$	$p\ [Pa]$	$\dot{m}_{ideal}\ [kg/s]$	$\dot{m}_{actual}\ [kg/s]$	C_D
1.00E-03	2.25E+00	9.61E+04	9.26E+04	2.40E-02	5.84E-03	2.43E-01
2.00E-03	1.12E+00	9.62E+04	9.15E+04	2.75E-02	1.25E-02	4.53E-01
3.00E-03	1.12E+00	9.63E+04	9.02E+04	4.67E-02	1.86E-02	3.97E-01
4.00E-03	1.12E+00	9.61E+04	8.96E+04	6.38E-02	2.24E-02	3.51E-01
5.00E-03	1.11E+00	9.63E+04	9.21E+04	6.49E-02	2.64E-02	4.06E-01
7.00E-03	1.12E+00	9.64E+04	9.14E+04	9.92E-02	3.31E-02	3.34E-01
1.00E-02	1.12E+00	9.65E+04	9.21E+04	1.33E-01	3.93E-02	2.95E-01

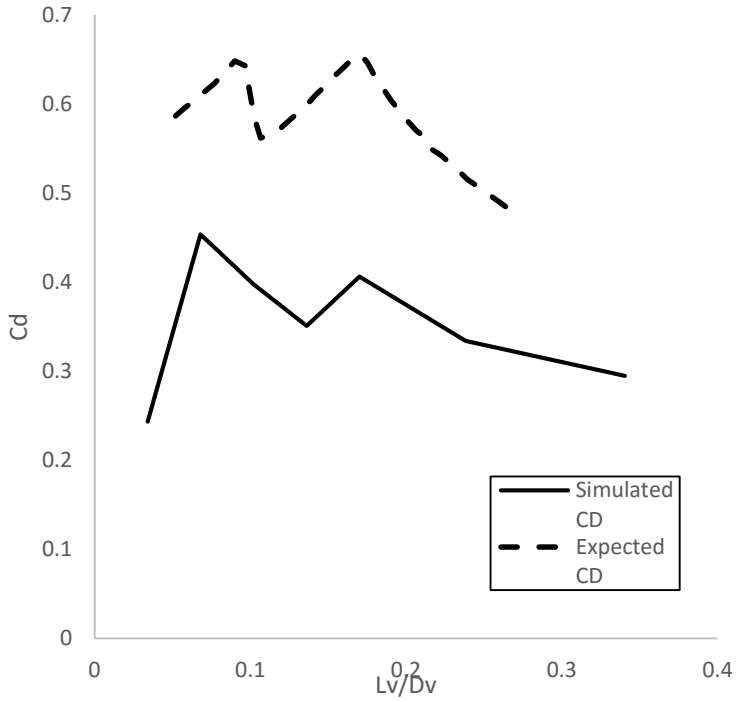

Figure A.13. Simulated CD values vs expected CD values.